Research article

NMR IN BIOMEDICINE

Received: 09 January 2013, Revised: 31 May 2013, Accepted: 10 June 2013, Published online in Wiley Online Library: 24 July 2013

(wileyonlinelibrary.com) DOI: 10.1002/nbm.2995

In vivo three-dimensional molecular imaging with Biosensor Imaging of Redundant Deviation in Shifts (BIRDS) at high spatiotemporal resolution

Daniel Coman[a,b,c]*, Robin A. de Graaf[a,c,d], Douglas L. Rothman[a,b,c,d] and Fahmeed Hyder[a,b,c,d]*

Spectroscopic signals which emanate from complexes between paramagnetic lanthanide (III) ions (e.g. Tm^{3+}) and macrocyclic chelates (e.g. 1,4,7,10-tetramethyl-1,4,7,10-tetraazacyclododecane-1,4,7,10-tetraacetate, or $DOTMA^{4-}$) are sensitive to physiology (e.g. temperature). Because nonexchanging protons from these lanthanide-based macrocyclic agents have relaxation times on the order of a few milliseconds, rapid data acquisition is possible with chemical shift imaging (CSI). Thus, Biosensor Imaging of Redundant Deviation in Shifts (BIRDS) which originate from nonexchanging protons of these paramagnetic agents, but exclude water proton detection, can allow molecular imaging. Previous two-dimensional CSI experiments with such lanthanide-based macrocyclics allowed acquisition from ~12-μL voxels in rat brain within 5 min using rectangular encoding of *k* space. Because cubical encoding of *k* space in three dimensions for whole-brain coverage increases the CSI acquisition time to several tens of minutes or more, a faster CSI technique is required for BIRDS to be of practical use. Here, we demonstrate a CSI acquisition method to improve three-dimensional molecular imaging capabilities with lanthanide-based macrocyclics. Using $TmDOTMA^{-}$, we show datasets from a $20 \times 20 \times 20$-mm^3 field of view with voxels of ~1 μL effective volume acquired within 5 min (at 11.7 T) for temperature mapping. By employing reduced spherical encoding with Gaussian weighting (RESEGAW) instead of cubical encoding of *k* space, a significant increase in CSI signal is obtained. *In vitro* and *in vivo* three-dimensional CSI data with $TmDOTMA^{-}$, and presumably similar lanthanide-based macrocyclics, suggest that acquisition using RESEGAW can be used for high spatiotemporal resolution molecular mapping with BIRDS.

Supporting information may be found in the online version of this paper

Keywords: methyl protons; chemical shift imaging; lanthanide; thulium; temperature; BIRDS; *k* space; rat brain

INTRODUCTION

Lanthanide-based complexes are widely used as MRI contrast agents as a result of their ubiquitous effect on water relaxation, mainly because of the paramagnetic ionic core in the molecular probe. However, MRS signals which emanate from these probes (i.e. not their effect on water) are also quite sensitive to physiology (e.g. temperature and/or pH). Based on the possibility that the acquisition of these paramagnetically shifted signals could have potential for molecular imaging, we have shown recently that Biosensor Imaging of Redundant Deviation in Shifts (BIRDS) which originate from these molecular probes can be used for pH and/or temperature mapping in rat brain (1,2). The BIRDS method is based on the strong dependence of temperature and/or pH on the chemical shifts of protons (or other nuclei) from complexes between lanthanide (III) ions (e.g. Tm^{3+}) and macrocyclic chelates of 1,4,7,10-tetraazacyclododecane-*N*,*N*′,*N*″,*N*‴-tetra (methylene phosphonate) ($TmDOTP^{5-}$) and 1,4,7,10-tetramethyl-1,4,7,10-tetraazacyclododecane-1,4,7,10-tetraacetate ($TmDOTMA^{-}$). Because the nonexchanging protons of paramagnetic agents (i.e., composed of lanthanide and transitional metail ions) have relaxation times on the order of just a few milliseconds, very fast data acquisition is achievable with conventional chemical shift imaging (CSI).

* *Correspondence to: F. Hyder/D. Coman, N135 TAC (MRRC), 300 Cedar Street, Yale University, New Haven, CT 06520, USA.*
E-mail: fahmeed.hyder@yale.edu, daniel.coman@yale.edu

a *D. Coman, R. A. Graaf, D. L. Rothman, F. Hyder*
Magnetic Resonance Research Center (MRRC), Yale University, New Haven, CT, USA

b *D. Coman, D. L. Rothman, F. Hyder*
Core Center for Quantitative Neuroscience with Magnetic Resonance (QNMR), Yale University, New Haven, CT, USA

c *D. Coman, R. A. Graaf, D. L. Rothman, F. Hyder*
Department of Diagnostic Radiology, Yale University, New Haven, CT, USA

d *R. A. Graaf, D. L. Rothman, F. Hyder*
Department of Biomedical Engineering, Yale University, New Haven, CT, USA

Abbreviations used: *BIRDS, Biosensor Imaging of Redundant Deviation in Shifts; CSI, chemical shift imaging; 2D/3D, two-/three-dimensional; $DOTMA^{4-}$, 1,4,7,10-tetramethyl-1,4,7,10-tetraazacyclododecane-1,4,7,10-tetraacetate; $DOTP^{5-}$, 1,4,7,10-tetraazacyclododecane-N,N′,N″,N‴-tetra(methylene phosphonate); FOV, field of view; PSF, point spread function; RF, radiofrequency; RESEGAW, reduced spherical encoding with Gaussian weighting; SLR, Shinnar–Le Roux; SNR, signal-to-noise ratio; TR, recycle time.*

Previous work with $TmDOTP^{5-}$ and $TmDOTMA^{-}$ in rat cerebral cortex used rectangular encoding of *k* space in conjunction with high-speed two-dimensional (2D) CSI at 11.7 T to allow the effective spatial resolution of 12.1 μL (nominal resolution of 10.2 μL) of BIRDS within 5 min of data acquisition (1,2). However, future applications of BIRDS may require whole-brain coverage and/or higher spatial resolution. For example, somatosensory stimulation, depending on the type of anesthesia and/or stimuli, leads to cortical activation volumes in the range 5–30 μL (3,4), and thus localized temperature mapping during functional activation (5) would require the fast acquisition of relatively small CSI voxels. Moreover, for selective brain cooling experiments (6–9), it is important to know the effectiveness of temperature lowering within a region, as well as throughout the whole brain, thereby requiring three-dimensional (3D) CSI of the whole brain with small voxels. All of these requirements are currently unachievable with present 2D CSI technology. For these types of experiments with BIRDS, a CSI method capable of 3D coverage of the entire rat brain with a spatial resolution of several microliters is required. As cubical encoding of *k* space in three dimensions increases the CSI acquisition time to several tens of minutes, we require a faster 3D CSI technique for practical use with BIRDS.

The replacement of cubical encoding with uniform spherical encoding of *k* space (10) reduces significantly the time of measurement, but results in an increase in the effective voxel volume. Moreover spherical encoding is preferred because it reduces the amplitude of Gibbs ringing (10,11). Spherical encoding of *k* space has been applied successfully in human calf muscle and human breast to obtain 3D ^{31}P CSI datasets at 7 T using an adiabatic multi-echo spectroscopic imaging pulse sequence (12). A spherical stack of spiral trajectories in *k* space was used to achieve reduced loss of spatial information in single-shot, whole-brain imaging, relative to acquisitions using concentric shell trajectories (13). Higher signal-to-noise ratio (SNR) and higher contrast-to-noise ratio within a shorter scan time were obtained using spherical *k*-space encoding with a 3D stack-of-rings trajectory relative to 3D Cartesian encoding (14).

Sensitivity per unit time can be improved by introducing the weighting of *k* space, in which less time is spent acquiring high *k*-space coordinates without a large loss of pixel resolution as a result of optimization of the point spread function (PSF) (11,15,16). Moreover, a smoother *k*-space weighting function decreases significantly Gibbs ringing artifacts (15). The optimal filter for maximum ripple reduction with minimum effect on the PSF is given by the Dolph–Chebyshev window function (17). However, a more widely used window function is the Hamming function, which represents a good approximation of the Dolph–Chebyshev window function (17). A Gaussian window function represents another commonly used window function to provide improved SNR and data collection efficiency (11) with reduced Gibbs ringing (18). Weighting of *k* space can also be achieved by making recycle time (TR) dependent on the *k*-space position, resulting in a significant reduction in measurement time (19). A significant reduction in measurement time can also be achieved by compressed sensing acquisitions, in which an appropriate nonlinear recovery scheme is used to recover images with a sparse representation obtained from randomly undersampled *k*-space acquisitions (20). Although *k*-space weighting provides some advantages relative to uniform encoding, the method is applicable only when signal averaging is required (e.g. ^{31}P CSI or ^{1}H CSI requiring more than one average).

In this study, we employed a 3D CSI method in which the temporal resolution was kept at 5 min using reduced spherical encoding with Gaussian weighting (RESEGAW) of *k* space, allowing us to achieve an effective voxel resolution of ~1 μL. The feasibility of obtaining temperature maps at high spatiotemporal resolution in rat brain was demonstrated with $TmDOTMA^{-}$ as a temperature sensor (Fig. 1A), because of the high SNR of its $-CH_3$ group (1).

MATERIALS AND METHODS

Construction of a 3D sampling function for an effective resolution of 1 μL

The estimation of the effective volume of a voxel was obtained by calculating the PSF for the cubical encoding and RESEGAW of *k* space. For the $29 \times 29 \times 29$ cubical encoding (Fig. 1B, inset), a 3D sampling function of *k* space was constructed, with unity assigned to all values. However, for RESEGAW, the proposed sampling function $G(R)$ was constructed using a Gaussian distribution of *k*-space sampling, with the maximum number of scans (N_C) in the center of *k* space (Fig. 1C):

$$G(R) = N_C e^{-\left(\frac{R}{R_d}\right)^2} \quad [1]$$

where R_d determines the width of the $G(R)$ distribution and R represents the distance from the center of *k* space to a *k*-space position described by the indices n_x, n_y and n_z in the three encoding directions:

$$R = \sqrt{n_x^2 + n_y^2 + n_z^2} \quad [2]$$

The $G(R)$ distribution was rounded to the closest integer value and, for encoding steps corresponding to $G(R) < 1$, a minimum value of one scan was assigned (Fig. 1C). However, based on spectral analysis of the 3D CSI dataset with $29 \times 29 \times 29$ cubical encoding (Fig. 1B), the encoding steps corresponding to $R > 14$ have negligible contribution to the total signal (Supporting information Fig. S1). Therefore, $G(R)$ was set to zero for encoding steps corresponding to $R > 14$, resulting in a 'spherical' encoding of *k* space (Fig. 1D, inset).

The PSF (normalized to unity) was obtained for both cubical (Fig. 1B) and RESEGAW (Fig. 1D) datasets by spatial Fourier transformation of the sampling function zero filled to a higher resolution ($257 \times 257 \times 257$). The effective volume of a voxel was calculated by counting the number of PSF points which have a normalized intensity larger than 0.5, (18). For example, for a 1D PSF, this number provides the width at half-maximum (Fig. 1B, D), whereas, for a 2D (or 3D) PSF, this number provides the area (or volume) at half-maximum. As the height of the PSF is normalized to unity and the volume of each PSF point can be expressed in volume units (μL), the number of PSF points with an intensity larger than 0.5 provides the effective volume of a voxel.

In vitro ^{1}H CSI

The 3D CSI datasets of a phantom containing 5 mM $TmDOTMA^{-}$ were obtained on a modified 11.7-T Agilent (Santa Clara, CA) horizontal-bore spectrometer using a ^{1}H resonator/surface radiofrequency (RF) probe (1.4 cm). Two 3D CSI datasets were acquired, one with cubical encoding (24 389 steps, Fig. 2A) and the

NMR IN BIOMEDICINE

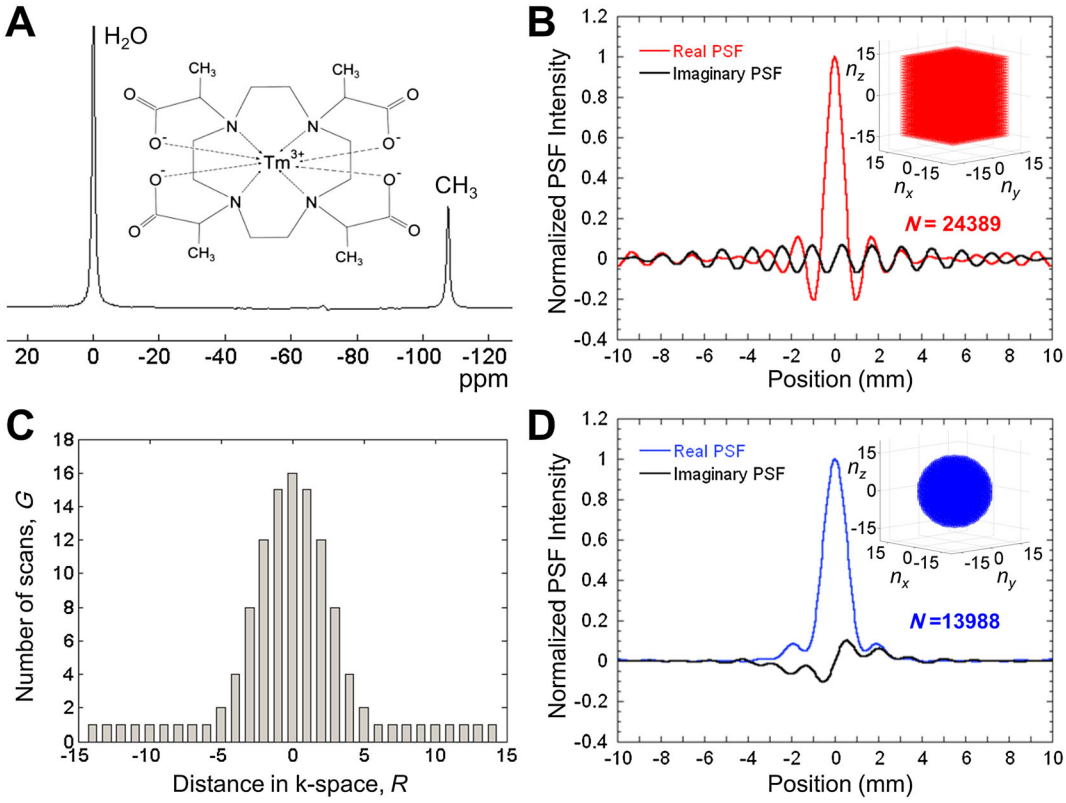

Figure 1. *In vitro* three-dimensional chemical shift imaging (3D CSI) with thulium 1,4,7,10-tetramethyl-1,4,7,10-tetraazacyclododecane-1,4,7,10-tetraacetate (TmDOTMA⁻). (A) Structure and ^{1}H spectrum of TmDOTMA⁻. (B) The real and imaginary parts of the point spread function (PSF) for $29 \times 29 \times 29 = 24\,389$ cubical encoding along one dimension (the other two directions have coordinates of zero). The effective voxel volume estimated using the 3D PSF for cubical encoding is 0.33 μL. (C) For reduced spherical encoding with Gaussian weighting (RESEGAW), the number of scans acquired for each *k*-space point follows a Gaussian distribution based on its distance *R* to the center of *k* space. (D) The real and imaginary parts of the PSF for RESEGAW with 13 988 steps along one dimension (the other two directions have coordinates of zero). The effective voxel volume estimated using the 3D PSF for RESEGAW is 1.0 μL. Thus, the acquisition of 3D CSI maps using RESEGAW results in a three-fold increase in the voxel effective volume relative to cubical encoding, but decreases the acquisition time by ~40%.

other with RESEGAW (13 988 steps, Fig. 2B). A single-banded refocused 90° Shinnar–Le Roux (SLR) RF pulse with a bandwidth of 40 kHz and a duration of 205 μs was used for selective excitation of the $-CH_3$ group of TmDOTMA⁻ (1). The datasets were acquired with a TR o ms and a field of view (FOV) of $20 \times 20 \times 20$ mm^3. The phase encode gradient duration was 100 μs and the acquisition time of the free induction decay was 4.1 ms. The spectrum for each encoding step was line broadened (300 Hz), phased (zero order) and baseline corrected (first order). The 3D CSI maps were obtained by spatial Fourier transformation of *k*-space spectra using these two CSI datasets.

In vivo ^{1}H CSI

All animal experimental procedures on rats were approved by the Institutional Animal Care and Use Committee and were similar to the procedures described previously (1,2,9). Sprague–Dawley rats ($n = 4$; 200–300 g) were tracheotomized and artificially ventilated (70% N_2O, 30% O_2). Isoflurane (3%) was used for induction and surgery. An intraperitoneal line was inserted for the administration of α-chloralose (46 ± 4 mg/kg/h) and an intravenous line was used for the administration of D-tubocurarine chloride (1 mg/kg/h) and TmDOTMA⁻ (0.5 mmol/kg). The infusion rate was adjusted to keep the animal within the autoregulatory range of cerebral perfusion. An arterial line was used to monitor physiology (blood pH, pO_2, pCO_2) throughout the experiment. The anesthetized rats were renally ligated. A water-heating blanket was used to control and maintain the body temperature. The *in vivo* 3D CSI acquisition and processing parameters were the same as those for the *in vitro* experiments (see above). The temperature *T* was calculated from the chemical shift of the $-CH_3$ protons (δ_{CH_3}) according to:

$$T = a_0 + a_1(\delta_{CH_3} - \delta_0) + a_2(\delta_{CH_3} - \delta_0)^2 \quad [3]$$

where $\delta_0 = -103.0$ ppm and the coefficients a_0 (34.45 ± 0.01), a_1 (1.460 ± 0.003) and a_2 (0.0152 ± 0.0009) were calculated from a linear least-squares fit of temperature as a function of the chemical shift δ_{CH_3}, as described previously (1).

RESULTS

Comparison of cubical encoding and RESEGAW

As the detailed analysis of the ^{1}H spectrum of TmDOTMA⁻ has been demonstrated previously (1), only a brief summary follows. Of the four detectable proton resonances, the $-CH_3$ group has the highest SNR relative to other ^{1}H signals which emanate from this molecular probe (Fig. 1A). Moreover, the chemical shift of the $-CH_3$ group shows high temperature sensitivity (0.7 ppm/° C) and very short relaxation times (i.e. T_1 and T_2 of less than 5

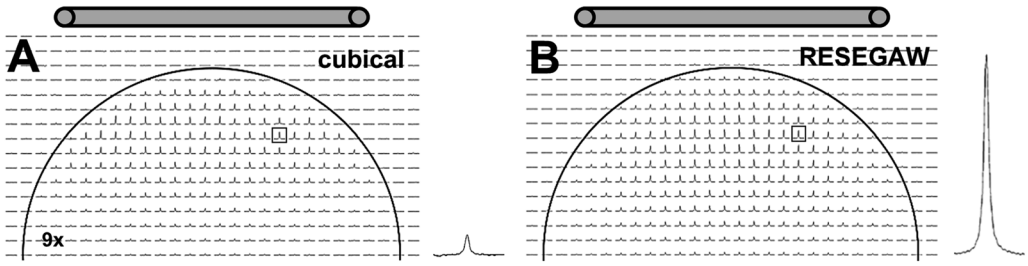

Figure 2. *In vitro* comparison between three-dimensional chemical shift imaging (3D CSI) with cubical encoding *versus* reduced spherical encoding with Gaussian weighting (RESEGAW) of *k* space with thulium 1,4,7,10-tetramethyl-1,4,7,10-tetraazacyclododecane-1,4,7,10-tetraacetate ($TmDOTMA^-$). (A) Example of a ^1H CSI slice ($z = 0$) obtained using cubical encoding. The spectrum on the right of the CSI dataset shows the signal of the $-CH_3$ resonance from the voxel boxed in the CSI dataset. (B) The same ^1H CSI slice as in (A) obtained using RESEGAW. The spectrum on the right of the CSI dataset shows the signal of the $-CH_3$ resonance in the same voxel as in (A). The CSI spectral intensities of the cubical dataset were multiplied by a factor of nine to match that of the RESEGAW dataset. The location of the surface coil relative to the phantom is also indicated by the gray horizontal cylindrical bar.

ms). Together, these reasons enable high-SNR molecular imaging for $TmDOTMA^-$ with high spatiotemporal BIRDS (1).

The acquisition of a cubical $29 \times 29 \times 29$ 3D CSI dataset requires 24 389 encoding steps, where each of the three orthogonal indices of *k* space (n_x, n_y, n_z) is incremented sequentially (by 1 from -14 to 14) with maximum intensity in the center of *k* space (18). Spectral analysis for all 24 389 encoding steps before spatial 3D Fourier transformation indicates that the intensity of the $-CH_3$ group is higher near the center of *k* space and decreases steeply away from the *k*-space center as *R* becomes larger (Fig. S1). As a result, the encoding steps corresponding to $R > R_0$, where $R_0 = 14$ represents the cut-off distance (indicated by the arrow in Fig. S1), have negligible contribution to the total signal, thereby suggesting that the acquisition of these data points in the case of the spherical encoding of *k* space may be avoided without compromising SNR significantly. However, this will reduce the number of encoding steps acquired. Thus, for uniform spherical encoding with $R < R_0$, the number of encoding steps can be decreased from 24 389 (Fig. 1B) to 12 770, whereas the addition of Gaussian weighting of spherical *k* space increases slightly the number of encoding steps to 13 988 (Fig. 1C, D). The reduction in the number of encoding steps from cubical $29 \times 29 \times 29$ 3D CSI to uniform spherical encoding results in a decrease of 48% in the experimental time, whereas the inclusion of the additional 1218 encoding steps to achieve Gaussian weighting of spherical *k* space results in an increase in the experimental time of 5%. Thus, the RESEGAW scheme requires only 57% of the experimental time of a cubical $29 \times 29 \times 29$ 3D CSI encoding scheme.

However, reduced sampling of *k* space has a detrimental effect on the effective volume of a voxel. Thus, the calculation of the corresponding PSF for each of the three *k*-space encoding schemes shows that the width of the PSF increases when the number of encoding steps is decreased. To exemplify this effect, the profile of the real and imaginary parts of the PSF along one of the three directions (corresponding to coordinate zero for the other two directions) was calculated for $29 \times 29 \times 29$ cubical (Fig. 1B; red, real PSF; black, imaginary PSF) and RESEGAW (Fig. 1D; blue, real PSF; black, imaginary PSF) datasets. Using these two PSFs, the effective voxel volume in each case was estimated (see Materials and Methods). Our calculations indicate that, for a FOV of 20 mm, the effective volume increases from 0.33 μL for cubical encoding to 0.75 μL for uniform spherical encoding and to 1.0 μL for RESEGAW. In addition, PSF calculation for a reduced $15 \times 15 \times 15$ cubical *k* space indicates that the effective voxel volume increases to 2.37 μL, although the experimental time is reduced by 86% compared with the $29 \times 29 \times 29$ cubical encoding. Moreover, the use of a reduced $15 \times 15 \times 15$ cubical encoding scheme results in enhanced Gibbs ringing artifacts. Therefore, 3D CSI with RESEGAW represents a compromise between spatial and temporal resolution in order to keep the temporal resolution to a reasonable value (5 min) with high SNR.

To compare the cubical and RESEGAW 3D CSI acquisitions *in vitro*, we calculated the ratio ρ between the signal intensity of RESEGAW and cubical datasets for 1251 voxels for which the signal was larger than 40% of the maximum signal in the cubical dataset. The average signal ratio over all of these voxels was $\rho = 9.3 \pm 2.3$. To further exemplify this result, we extracted the central CSI slice corresponding to position $z = 0$ for the cubical (Fig. 2A) and RESEGAW (Fig. 2B) datasets. The signal of the cubical dataset was increased nine-fold (Fig. 2A) to match that of the RESEGAW dataset (Fig. 2B). Moreover, comparison of the signal intensity in the same CSI voxel from the two CSI datasets indicates almost a 10-fold intensity enhancement for the RESEGAW acquisition (Fig. 2A, B, right). However, the effective volume of a voxel in RESEGAW is three-fold larger than that for cubical encoding. Therefore, the enhancement factor per unit of volume is 3.1 (=9.3/3), indicating that the signal for RESEGAW is about three-fold larger than for cubical encoding. This increase in the signal is probably caused by the shape of the RESEGAW PSF, which is mostly positive (Fig. 1D), compared with a more sinc-like shape with alternating positive and negative contributions for cubical encoding (Fig. 1B). The effective voxel volume is calculated at 50% of the PSF (which is a common way to calculate the PSF), but the entire PSF contributes to the MR signal. Thus, although the PSF for cubical encoding stretches on forever, but is largely self-canceling (Fig. 1B), the PSF for RESEGAW is much more localized, but is all positive (Fig. 1D). Moreover, acquisition of a RESEGAW dataset is 1.7-fold (=24 389/13 988) faster than that of a cubical 3D CSI dataset. These results suggest that RESEGAW should be preferable than cubical encoding when acquiring 3D CSI for BIRDS.

In vivo 3D CSI with RESEGAW

To demonstrate the *in vivo* feasibility of acquiring 3D CSI experimental data with high spatiotemporal resolution, datasets of rat brain with a FOV of 20 mm in each direction were obtained using RESEGAW of *k* space with 13 988 encoding steps, similar to the *in vitro* data shown in Fig. 2. The 13 988 encoding steps were acquired in less than 5 min using TR = 10 ms and two averages.

To exemplify 3D CSI mapping of rat brain, spectra from three CSI slices positioned at +0.7, –2.8 and −6.2 mm from the bregma are shown at the top, middle and bottom, respectively, of Fig. 3. The chemical shift of the $-CH_3$ group of TmDOTMA⁻ was measured in each voxel, and Equation ([3]) was used to calculate the temperature distribution in each slice. The three maps, overlaid on the CSI datasets, show a relatively homogeneous temperature distribution in rat cerebral cortex, with average temperatures of 36.4 ± 0.3, 36.5 ± 0.2 and 36.3 ± 0.3 °C for the three slices. Temperature measurements over the entire brain indicate a relatively symmetrical distribution, with an average value of 36.4 ± 0.6 °C. The temperature values span a relatively narrow range, with 85% of the values between 36 and 37 °C (Supporting information Fig. S2). However, closer inspection of smaller regions shows heterogeneity across cortical layers and the inner core of the brain (e.g. corpus callosum, hippocampus, superior colliculus), as shown in Fig. 3 and Table 1, where the temperature is progressively warmer from the outer surface to the deeper brain tissues.

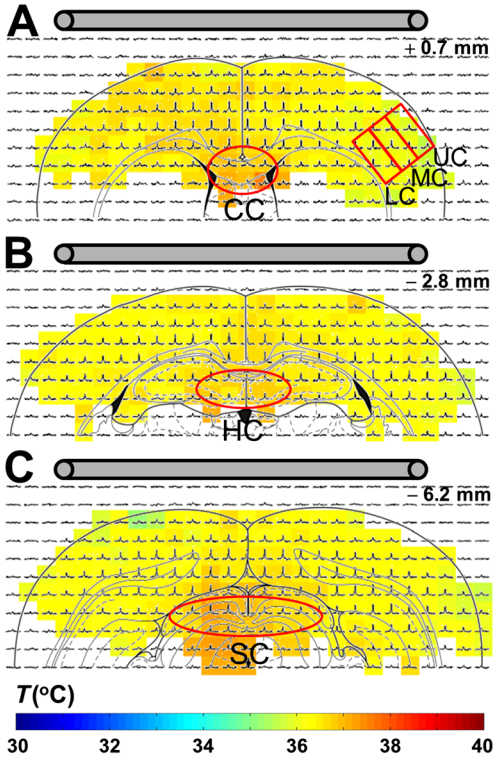

Figure 3. *In vivo* three-dimensional chemical shift imaging (3D CSI) with thulium 1,4,7,10-tetramethyl-1,4,7,10-tetraazacyclododecane-1,4,7,10-tetraacetate (TmDOTMA⁻) using reduced spherical encoding. Examples of three ^{1}H CSI slices from a 3D CSI reduced spherical encoding with Gaussian weighting (RESEGAW) dataset in rat brain, positioned at +0.7 mm (A), –2.8 mm (B) and −6.2 mm (C) from the bregma. The temperature distribution in the three slices was calculated using Equation [3]. The average temperatures were 36.4 ± 0.3, 36.5 ± 0.2 and 36.3 ± 0.3 °C, respectively. The presence of a temperature gradient of ~0.3 °C across the cortex was demonstrated by measuring the average temperatures in the upper (UC), middle (MC) and lower (LC) cortical layers, indicated by the three red boxes in (A). Moreover, significantly higher temperatures (>0.5 °C compared with the cortex) were measured in the corpus callosum [CC, red oval in (A)], hippocampus [HC, red oval in (B)] and superior colliculus [SC, red oval in (C)]. The location of the surface coil relative to the animal brain is also indicated by the gray horizontal cylindrical bar.

Table 1. Regional average temperatures measured in rat brain in the upper, middle and lower cortical layers (Fig. 3A, red boxes, UC, MC and LC), corpus callosum (Fig. 3A, red oval, CC), hippocampus (Fig. 3B, red oval, HC) and superior colliculus (Fig. 3C, red oval, SC)

Region	Average temperature (°C)[1]
Upper cortical layer	36.0 ± 0.2
Middle cortical layer	36.2 ± 0.2
Lower cortical layer	36.3 ± 0.2
Corpus callosum	36.8 ± 0.3
Hippocampus	36.8 ± 0.1
Superior colliculus	36.9 ± 0.2

[1] *t*-test analysis using two-tailed distribution with unequal variance indicates statistically significant differences with $p < 0.02$ when comparing the upper cortical layer with the other regions investigated.

DISCUSSION

In this work, we have reported the *in vivo* feasibility of obtaining high spatiotemporal resolution 3D CSI mapping of rat brain using a lanthanide macrocyclic complex, TmDOTMA⁻. Previous BIRDS experiments in our laboratory used TmDOTMA⁻ as a temperature sensor based on its high temperature sensitivity (0.7 ppm/°C) and very high SNR of the $-CH_3$ resonance (1). The 2D CSI data of a 4-mm slice were acquired using 16 × 16 encoding steps with a FOV of 25.6 × 25.6 mm^2, TR = 11 ms and 100 averages, thus resulting in a total acquisition time of 5 min and a nominal voxel volume of 10.2 μL (effective voxel volume of 12.1 μL). In the current study, we acquired high-SNR 3D CSI datasets with an effective voxel volume of 1 μL (nominal voxel volume of 0.33 μL) in 5 min using a reduced *k*-space spherical encoding with Gaussian weighting (named RESEGAW). The smaller number of averages required for the 3D CSI with RESEGAW experiment, compared with our previous 2D CSI experiments, was a consequence of signal acquisition from the entire animal brain. In addition, Gaussian weighting with increased averaging of encoding steps from the center of *k* space results in significant signal enhancement (Fig. 2). However, the effective voxel volume is three-fold larger (1 μL) compared with the nominal voxel volume (0.33 μL).

The determination of the number of *k*-space encoding steps with significant contribution to the total signal, involving the estimation of the cut-off distance R_0, depends on the distribution of signal intensity in *k* space. This distribution is dependent on various factors, such as the local agent concentration, shape and size of the sample investigated, FOV, etc. Thus, *in vitro* 3D CSI experiments were designed to closely mimic the *in vivo* situation. The spherical shape, size and location of the *in vitro* sample are similar to that of animal brain, leading to similar distributions of signal intensity in *k* space. Moreover, the *in vitro* agent concentration (5 mM) was similar to the estimated TmDOTMA⁻ concentration of about 3–4 mM in rat brain (1). The use of *in vitro* samples with higher TmDOTMA⁻ concentration would have resulted in a better SNR and thus a wider region of *k* space with significant contribution to the total signal. Therefore, based on the *in vitro* results, we expected that it would be possible to successfully apply the 3D CSI method with

RESEGAW to obtain 3D CSI datasets of rat brain. Indeed, the analysis of signal distribution in *k* space for the *in vivo* 3D CSI datasets indicate that a cut-off distance $R_0 = 14$ provides a good compromise between the desired fast acquisition (which requires a smaller number of encoding steps) and increased spatial resolution (which requires a larger number of encoding steps).

Extremely fast CSI data acquisition with a very short TR (10 ms) is possible because the T_1 value of $TmDOTMA^-$ is very short (<5 ms). However, this TR limit is spectrometer based, which, if reduced in the future, will significantly enhance the sensitivity of BIRDS, especially for agents with extremely short T_1 (e.g. smaller than 1 ms). Based on the previously measured T_2 value of 4.17 ms for the $TmDOTMA^-$ methyl group (1), the signal decay during phase encoding (0.1 ms) is only 2.5% of the signal, indicating that signal decay during phase encoding as a result of T_2 relaxation prior to free induction decay collection is minimal. Moreover, the short acquisition time of 4.1 ms does not produce any ringing artifacts in the spectrum of $TmDOTMA^-$.

Multi-slice 20×20 2D ^{1}H-[^{13}C] edited CSI experiments with a nominal voxel resolution of 1 μL (effective resolution of 1.7 μL) in microwaved rat brains have been performed previously to allow the generation of *ex vivo* metabolic maps of [4-^{13}C]-glutamate, [4-^{13}C]-glutamine and other ^{13}C-labeled molecules (21). The dynamics of lactate generation in focal ischemic rat brain were also estimated using ^{1}H-[^{13}C] edited CSI experiments with a nominal voxel resolution of 1.9 μL (effective resolution of 2.2 μL) (22). The detection of ^{13}C-labeled brain metabolites requires a relatively long TR (1.5 s or longer) which results in a long CSI experiment (30 min or more). Similarly, high-resolution quantitative ^{1}H metabolite maps of more than 10 metabolites from rat brain were obtained in ~1 h using a 2D CSI experiment with a nominal resolution of 1.1 μL and an effective voxel size of 1.7 μL (23). Although spectroscopic imaging of these metabolites can be speeded up significantly using echo-planar imaging schemes (24), whole-brain CSI maps would still require quite long acquisition times with superior outer volume suppression (25). Thus, the ^{1}H detection of signals from lanthanide-based macrocyclics, such as $TmDOTMA^-$, at high temporal resolution (~5 min) represents a direct consequence of their short T_1 and T_2 relaxation times, which are on the order of milliseconds (1,2,9).

The average brain temperature measured in this study, 36.4 ± 0.6 °C (Fig. S2), is slightly higher than our previous measurements, where average temperatures of 34.6 ± 0.4 and 34.8 ± 0.4 °C were estimated using 2D CSI of 4-mm slices with $TmDOTP^{5-}$ and $TmDOTMA^-$, respectively (1). However, this result can be easily explained by the strong correlation always observed between the brain and body temperatures (data not shown). Thus, in our previous measurements, the body temperatures of the rat during 2D CSI acquisition were 35.8 ± 0.1 and 36.1 ± 0.1 °C for $TmDOTP^{5-}$ and $TmDOTMA^-$, respectively, whereas, during the CSI acquisition with RESEGAW, the core temperature was 37.4 ± 0.1 °C. A very important consequence of obtaining high-resolution temperature maps in rat brain is that the measurement of temperature differences between various brain regions is now possible. These types of regional differences have been measured previously by thermocouple wires only (26). Temperature measurements in specific cortical regions indicate a gradual increase in the temperature by ~0.3 °C when going from upper to lower cortical layers (Fig. 3A, red boxes and Table 1). Moreover, average temperatures in the inner core of the brain were higher by more than 0.5 °C compared with the cortex (Table 1), as indicated by the 'warmer' colors in the corpus callosum (red oval in Fig. 3A), hippocampus (red oval in Fig. 3B) and superior colliculus (red oval in Fig. 3C).

The $TmDOTMA^-$ concentration during a typical *in vivo* experiment is about 3–4 mM in the blood and 3 mM in the extracellular space, as measured previously for the protocol used in the current study (1). This relatively high $TmDOTMA^-$ concentration achieved in the brain's extracellular space is a result of the increased blood–brain concentration gradient, which presumably helps to facilitate its passive diffusion. However, given the high SNR of 3D CSI data shown here, we believe that the $TmDOTMA^-$ infusion dose can be decreased. This method requires renal ligation. To overcome this surgical limitation, we are currently conducting studies to implement pharmacological means to temporarily inhibit renal clearance. Future biodistribution studies with surgical and pharmacological renal intervention could allow the detailed examination of how ubiquitously $TmDOTMA^-$ is distributed in different tissues. Previous studies from other laboratories have shown that agents similar to $TmDOTMA^-$ are widely distributed throughout the body (27,28). The relatively homogeneous biodistribution of these lanthanide-based agents suggests that BIRDS could be successfully applied not only for brain, but also for measurements in other organs.

RF or B_1 variations caused by the use of a surface coil (Figs 2 and 3) were observed in the $TmDOTMA^-$ intensity. This is precisely the reason why the $TmDOTMA^-$ signal is not observed further beyond the hippocampus or superior colliculus. However, no B_1 corrections were necessary as long as the chemical shift of $TmDOTMA^-$ could be measured accurately with sufficient SNR. Moreover, because T_2 of $TmDOTMA^-$ is extremely short (<5 ms), the $TmDOTMA^-$ signal is not significantly sensitive to static field inhomogeneity or B_0 shim effects, (i.e. linewidth of >100 Hz). The smaller intensities of $TmDOTMA^-$ at the top of the phantom (Fig. 2) and in the outermost layers of the cortex (Fig. 3) are caused by partial volume effects. However, these smaller intensities do not affect the results because the BIRDS estimate of temperature is only dependent on the chemical shift.

In summary, the current results demonstrate a significant improvement in 3D spatial resolution for BIRDS compared with the previously obtained 2D CSI experiments, whilst keeping the same temporal resolution at 5 min. 3D CSI acquisition with RESEGAW increases the spatial resolution by one order of magnitude by decreasing the effective voxel size from 12 to 1 μL. The acquisition of high spatiotemporal resolution isotropic 3D CSI datasets from whole rat brain has numerous applications for physiological imaging, such as functional activation during somatosensory stimulation and/or selective brain cooling. The high spatiotemporal resolution achieved with $TmDOTMA^-$, and presumably similar agents (1,2,9,29), demonstrates that 3D CSI acquisition with RESEGAW could be successfully used for molecular mapping with BIRDS.

Acknowledgements

The authors thank the scientists and engineers at the Magnetic Resonance Research Center (MRRC) (mrrc.yale.edu) and Core Center for Quantitative Neuroscience with Magnetic Resonance (QNMR) (qnmr.yale.edu), Yale University, New Haven, CT, USA. This work was supported by grants from the National Institutes of Health (R01 CA-140102, R01 EB-011968, P30 NS-52519).

REFERENCES

1. Coman D, Trubel HK, Hyder F. Brain temperature by Biosensor Imaging of Redundant Deviation in Shifts (BIRDS): comparison between $TmDOTP^{5-}$ and $TmDOTMA^-$. NMR Biomed. 2010; 23(3): 277–285.
2. Coman D, Trubel HK, Rycyna RE, Hyder F. Brain temperature and pH measured by (1)H chemical shift imaging of a thulium agent. NMR Biomed. 2009; 22(2): 229–239.
3. Sanganahalli BG, Herman P, Hyder F. Frequency-dependent tactile responses in rat brain measured by functional MRI. NMR Biomed. 2008; 21(4): 410–416.
4. Maandag NJ, Coman D, Sanganahalli BG, Herman P, Smith AJ, Blumenfeld H, Shulman RG, Hyder F. Energetics of neuronal signaling and fMRI activity. Proc. Natl. Acad. Sci. USA 2007; 104(51): 20 546–20 551.
5. Trubel HK, Sacolick LI, Hyder F. Regional temperature changes in the brain during somatosensory stimulation. J. Cereb. Blood Flow Metab. 2006; 26(1): 68–78.
6. Trubel H, Herman P, Kampmann C, Huth R, Maciejewski PK, Novotny E, Hyder F. A novel approach for selective brain cooling: implications for hypercapnia and seizure activity. Intensive Care Med. 2004; 30(9): 1829–1833.
7. Trubel H, Herman P, Kampmann C, Novotny E, Hyder F. Selective pharyngeal brain cooling. Biomed. Tech. (Berl.) 2003; 48(11): 298–300.
8. Trubel H, Herman P, Kampmann C, Novotny E, Hyder F. Duration of induced seizures during selective pharyngeal brain cooling. Biomed. Tech. (Berl.) 2004; 49(10): 279–281.
9. Trubel HK, Maciejewski PK, Farber JH, Hyder F. Brain temperature measured by ^{1}H-NMR in conjunction with a lanthanide complex. J. Appl. Physiol.. 2003; 94(4): 1641–1649.
10. Maudsley AA, Matson GB, Hugg JW, Weiner MW. Reduced phase encoding in spectroscopic imaging. Magn. Reson. Med. 1994; 31(6): 645–651.
11. Hugg JW, Maudsley AA, Weiner MW, Matson GB. Comparison of k-space sampling schemes for multidimensional MR spectroscopic imaging. Magn. Reson. Med. 1996; 36(3): 469–473.
12. van der Kemp WJM, Boer VO, Luijten PR, Stehouwer BL, Veldhuis WB, Klomp DWJ. Adiabatic multi-echo ^{31}P spectroscopic imaging (AMESING) at 7 T for the measurement of transverse relaxation times and regaining of sensitivity in tissues with short T_2* values. NMR Biomed. 2013; doi: 10.1002/nbm.2952.
13. Assländer J, Zahneisen B, Hugger T, Reisert M, Lee H-L, LeVan P, Hennig J. Single shot whole brain imaging using spherical stack of spirals trajectories. Neuroimage, 2013; 73(0): 59–70.
14. Wu HH, Nishimura DG. 3D magnetization-prepared imaging using a stack-of-rings trajectory. Magn. Reson. Med. 2010; 63(5): 1210–1218.
15. Parker DL, Gullberg GT, Frederick PR. Gibbs artifact removal in magnetic resonance imaging. Med. Phys. 1987; 14(4): 640–645.
16. Mareci TH, Brooker HR. Essential considerations for spectral localization using indirect gradient encoding of spatial information. J. Magn. Reson.. 1991; 92(2): 229–246.
17. Ernst RR, Bodenhausen G, Wokaun A. *Principles of Nuclear Magnetic Resonance in One and Two Dimensions*. Clarendon Press: Oxford; 1987.
18. de Graaf RA. *In vivo NMR Spectroscopy – Principles and Techniques*, 2nd edn. Wiley: Chichester, West Sussex; 2007.
19. Kuhn B, Dreher W, Norris DG, Leibfritz D. Fast proton spectroscopic imaging employing k-space weighting achieved by variable repetition times. Magn. Reson. Med. 1996; 35(4): 457–464.
20. Lustig M, Donoho D, Pauly JM. Sparse MRI: The application of compressed sensing for rapid MR imaging. Magn. Reson. Med. 2007; 58(6): 1182–1195.
21. de Graaf RA, Chowdhury GM, Brown PB, Rothman DL, Behar KL. In situ 3D magnetic resonance metabolic imaging of microwave-irradiated rodent brain: a new tool for metabolomics research. J. Neurochem. 2009; 109(2): 494–501.
22. Dijkhuizen RM, de Graaf RA, Garwood M, Tulleken KA, Nicolay K. Spatial assessment of the dynamics of lactate formation in focal ischemic rat brain. J. Cereb. Blood Flow Metab. 1999; 19(4): 376–379.
23. Mlynarik V, Kohler I, Gambarota G, Vaslin A, Clarke PG, Gruetter R. Quantitative proton spectroscopic imaging of the neurochemical profile in rat brain with microliter resolution at ultra-short echo times. Magn. Reson. Med. 2008; 59(1): 52–58.
24. Hyder F, Renken R, Rothman DL. In vivo carbon-edited detection with proton echo-planar spectroscopic imaging (ICED PEPSI): [3,4-(13)CH(2)]glutamate/glutamine tomography in rat brain. Magn. Reson. Med. 1999; 42(6): 997–1003.
25. Shungu DC, Glickson JD. Sensitivity and localization enhancement in multinuclear in vivo NMR spectroscopy by outer volume presaturation. Magn. Reson. Med. 1993; 30(6): 661–671.
26. Kiyatkin EA. Brain temperature fluctuations during physiological and pathological conditions. Eur. J. Appl. Physiol. 2007; 101(1): 3–17.
27. Woods M, Caravan P, Geraldes CF, Greenfield MT, Kiefer GE, Lin M, McMillan K, Prata MI, Santos AC, Sun X, Wang J, Zhang S, Zhao P, Sherry AD. The effect of the amide substituent on the biodistribution and tolerance of lanthanide(III) DOTA-tetraamide derivatives. Invest. Radiol. 2008; 43(12): 861–870.
28. Geraldes CF, Sherry AD, Lazar I, Miseta A, Bogner P, Berenyi E, Sumegi B, Kiefer GE, McMillan K, Maton F, Muller RN. Relaxometry, animal biodistribution, and magnetic resonance imaging studies of some new gadolinium (III) macrocyclic phosphinate and phosphonate monoester complexes. Magn. Reson. Med. 1993; 30(6): 696–703.
29. Coman D, Kiefer GE, Rothman DL, Sherry AD, Hyder F. A lanthanide complex with dual biosensing properties: CEST (chemical exchange saturation transfer) and BIRDS (biosensor imaging of redundant deviation in shifts) with europium DOTA-tetraglycinate. NMR Biomed.. 2011; 24(10): 1216–1225.